Mapping the chemical chromatin reactivation landscape identifies BRD4-TAF1 cross-talk

Sara Sdelci, Charles-Hugues Lardeau, Cynthia Tallant, Freya Klepsch, Björn Klaiber, James Bennett, Philipp Rathert, Michael Schuster, Thomas Penz, Oleg Fedorov, Giulio Superti-Furga, Christoph Bock, Johannes Zuber, Kilian V. M. Huber, Stefan Knapp, Susanne Müller, Stefan Kubicek*

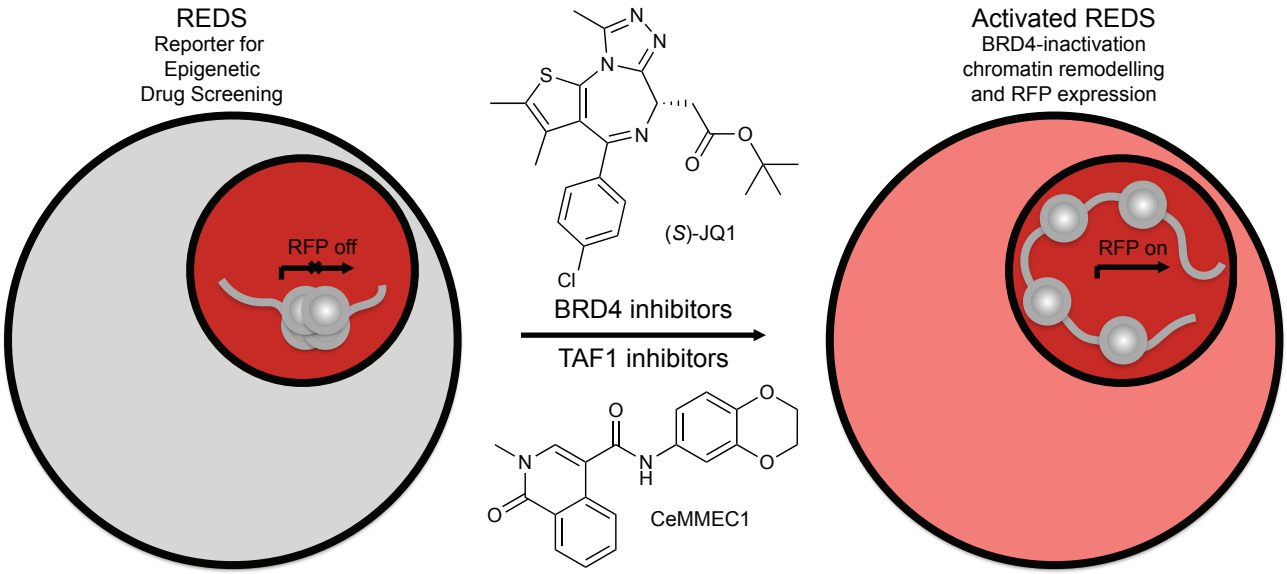

*To whom correspondence should be addressed:

Stefan Kubicek
CeMM Research Center for Molecular Medicine of the Austrian Academy of Sciences
Lazarettgasse 14, 1090 Vienna, Austria
Phone : +43-1-40160-70036, Fax: +43-1-40160-970 000,
Email: skubicek@cemm.oeaw.ac.at

Manuscript in press

Nature Chemical Biology manuscript NCHEMB-A151003020A

Submitted September 23, 2015
Revised January 11, 2016
Accepted March 16, 2016

Mapping the chemical chromatin reactivation landscape identifies BRD4-TAF1 cross-talk

Sara Sdelci[1], Charles-Hugues Lardeau[1,2], Cynthia Tallant[3], Freya Klepsch[1], Björn Klaiber[1], James Bennett[3], Philipp Rathert[4,5], Michael Schuster[1], Thomas Penz[1], Oleg Fedorov[3], Giulio Superti-Furga[1,6], Christoph Bock[1,7,8], Johannes Zuber[4], Kilian V. M. Huber[1,3], Stefan Knapp[3,9], Susanne Müller[3], Stefan Kubicek[1,2,*]

[1]CeMM Research Center for Molecular Medicine of the Austrian Academy of Sciences. Lazarettgasse 14, 1090 Vienna, Austria
[2]Christian Doppler Laboratory for Chemical Epigenetics and Antiinfectives, CeMM Research Center for Molecular Medicine of the Austrian Academy of Sciences, Vienna, Austria.
[3]Structural Genomics Consortium and Target Discovery Institute, Nuffield Department of Clinical Medicine, University of Oxford, Oxford, UK
[4]Research Institute of Molecular Pathology (IMP), Vienna Biocenter (VBC), 1030 Vienna, Austria
[5]Present address: Institute of Biochemistry, University Stuttgart, Stuttgart, Germany
[6]Center for Physiology and Pharmacology, Medical University of Vienna, Vienna, Austria
[7]Department of Laboratory Medicine, Medical University of Vienna, 1090 Vienna, Austria
[8]Max Planck Institute for Informatics, 66123 Saarbrücken, Germany
[9]Johann Wolfgang Goethe-University, Institute for Pharmaceutical Chemistry and Buchmann Institute for Life Sciences, Max-von-Laue-Str. 9, D-60438 Frankfurt am Main, Germany

*To whom correspondence should be addressed:

Stefan Kubicek
CeMM Research Center for Molecular Medicine of the Austrian Academy of Sciences.
Lazarettgasse 14, 1090 Vienna, Austria
Phone : +43-1-40160-70036, Fax: +43-1-40160-970 000,
Email: skubicek@cemm.oeaw.ac.at

ABSTRACT

Bromodomain proteins of the BET family recognize histone lysine acetylation and mediate transcriptional activation of target genes such as the *c-MYC* oncogene. Pharmacological BET domain inhibitors promise therapeutic benefits in a variety of cancers. We performed a high-diversity chemical compound screen for agents able to modulate BRD4-dependent heterochromatization of a generic reporter in human cells. On top of known and new compounds targeting BRD4, we identified small molecules that mimic BRD4 inhibition without direct engagement. One such compound was a potent inhibitor of the second bromodomain of TAF1. Using this inhibitor, we discovered that TAF1 synergizes with BRD4 to control cancer cell proliferation, making TAF1 an attractive epigenetic target in *c-MYC* driven cancers.

INTRODUCTION

BRD4 (bromodomain-containing protein 4) is an acetyl-lysine reader of the BET (bromodomain and extraterminal domain) family[1–3]. This protein binds to acetylated histones at promoter and enhancer regions and recruits transcription factors, cofactors and RNA polymerase II (RNApol II), thus modulating the transcription of a subset of genes in a highly context dependent way. Through its effect on chromatin structure, genomic stability[4,5] and target gene expression[6,7], the bromodomain-histone interaction plays a key role regulating cell cycle progression[2,5,8], and contributes to several pathologies including cancer[6,8–10]. The design of chemical probe compounds targeting the two bromodomains of BRD4, such as the pan-BET inhibitors JQ1[11] and I-BET-151[12] and their compelling efficacy in cancer models, has prompted the development of drug candidates for these protein interaction modules that are now undergoing clinical trials[13].

Despite the large number of competing clinical programs, the mechanistic and chemical diversity of currently available BRD4 inhibitors is limited[3,13]. Furthermore, we lack a detailed understanding of the factors affecting BRD4 function. We set out to design a strategy allowing the unbiased scouting of high diversity chemical space for modulators of a BRD4-dependent inactive chromatin state. In the background of the human haploid cell line KBM7[14], allowing unambiguous monoallelic genetic configurations, we integrated the RFP (Red Fluorescent Protein) gene in heterochromatic loci which are specifically activated by BRD4 inhibition. We then chose a high-diverse compound library of 89,355 small molecules and selected compounds for their ability to reactivate RFP expression. The efficient identification of many BRD4 inhibitors, including all the BET inhibitors in our library, validated the experimental strategy. Importantly, the setup allowed the identification of small molecules that efficiently induced RFP expression but failed to bind BRD4, suggesting a novel mechanism of action. We were able to show that one such compound functioned by binding the second bromodomain of the transcription initiation factor TAF1. Investigation of the properties of this new compound and its derivatives enabled us to demonstrate a strong synergy between the targeting of TAF1 and BRD4, which resulted in efficient killing of BRD4-dependent cancer cells.

RESULTS

A cellular reporter for functional BRD4 inhibition

We aimed to generate a cellular reporter system that rapidly responds to epigenetic changes with a gain of signal and is optimally suited to both chemical and genetic screens. Therefore, we developed a strategy of targeting a reporter construct to heterochromatic loci in KBM7 cells, a chronic myeloid leukaemia cell line with a near-haploid karyotype[14] (**Fig. 1a**). To identify such BRD4-repressed loci in an unbiased way, we pre-incubated KBM7 cells with the potent and selective BET bromodomain inhibitor (*S*)-JQ1 at a concentration that was sufficient to provoke chromatin reorganization, *c-MYC* repression (**Supplementary Results, Supplementary Fig. 1a**) and partial cell cycle arrest, while not causing apoptosis (**Supplementary Fig. 1b**). We then infected (*S*)-JQ1-treated cells with a retrovirus for the expression of RFP and applied a strategy of double FACS sorting to obtain a population of cells that express RFP in the presence of (*S*)-JQ1 and repress the transgene after withdrawal of the compound (**Fig. 1a** and **Fig. 1b**).

We isolated three clones as Reporters for Epigenetic Drug Screening (REDS1, REDS2 and REDS3), which expressed RFP in response to (*S*)-JQ1 (**Supplementary Fig. 1c**). Because of its strong and uniform RFP intensity, clone REDS3 was selected for further validation and experiments. The treatment of REDS3 cells with (*S*)-JQ1 induced a clear and robust increase of RFP expression detected by flow cytometry (**Fig. 1c**), live cell imaging (**Supplementary Fig. 1c**) and real time PCR (RT-PCR) (**Supplementary Fig. 1d**). In addition to RFP, the zeocin resistance gene present on the retroviral vector was also upregulated (RT-PCR data, **Supplementary Fig. 1e**). Moreover, RFP expression was not caused by the partial cell cycle arrest induced by (*S*)-JQ1, as the synchronization of REDS3 in different phases of the cell cycle did not increase the number of RFP-positive cells (**Supplementary Fig. 1f**). Recently, the activation of the LTR (Long Terminal Repeat) of HIV-1 (Human Immunodeficiency Virus-1) has been reported to be stimulated by (*S*)-JQ1, and the inhibition of BRD4 potentiates the action of known transcriptional HIV-1 reactivating compounds, such as PMA (phorbol myristate acetate) or PHA (phytohemagglutinin)[15,16]. To rule this out as a possible mechanism of RFP expression, REDS3 cells were treated with PMA, PHA or a

combination of each of these compounds with (*S*)-JQ1. No increase of RFP-positive nuclei was observed with these compounds (**Supplementary Fig. 1g**). Therefore, RFP expression was likely due to the effect of (*S*)-JQ1 on the locus of insertion rather than the inserted LTR.

(*S*)-JQ1, like almost all BRD4 inhibitors, targets the entire BET bromodomain family (BRD2, BRD3, BRD4, BRDT) with comparable potency in addition to very weak interaction with a few other human bromodomains[11]. To clarify which BET target is responsible for RFP repression and rule out off-target effects, we knocked down all the (*S*)-JQ1 targets individually in the REDS3 clone and quantified RFP-positive cells by flow cytometry. Only the downregulation of BRD4 resulted in an increase of RFP-positive nuclei (**Fig. 1d**). This effect was also visible by live cell imaging (**Fig. 1e**) and accompanied by increased levels of RFP mRNA, not observed for instance following BRD3 downregulation (**Supplementary Fig. 1h**). Thus, we have been able to create an experimental system allowing for a focused phenotypic screen for perturbations, be they genetic, pharmacological or metabolic, resulting in release from the BRD4-driven heterochromatin state.

To further validate the REDS3 clone, we performed FISH (fluorescence in situ hybridization) and confirmed the presence of a single RFP insertion per cell (**Fig. 1f**). The RFP probe was preferentially located in proximity to the nuclear membrane (**Fig. 1g**), suggesting RFP heterochromatin localization[17,18]. We used a sequencing approach to map the RFP locus to region 12q24.33, located less than 3 Mb from the telomere of chromosome 12 (**Supplementary Fig. 2a**). The sequencing data were confirmed by PCR using specific pairs of genomic primers for wild-type (WT) and REDS3 KBM7 cells (**Supplementary Fig. 2b**). Less than 5 kb upstream of the *RFP* insertion is the *STX2* gene, which is lowly expressed in KBM7 (RNA-seq (RNA sequencing) data; RPKM <1) and flanked by heterochromatin regions[19]. In contrast, the gene *RAN*, located 35 kb downstream of the RFP locus, is robustly expressed in KBM7 and has previously been described as a BRD4 target gene[9]. Interestingly, the region between STX2 and RAN is enriched in repeated enhancer sequences (ENCODE), endorsing the hypothesis of a super-enhancer[20] controlling the expression of *RAN*. Even though BRD4 has been considered a transcriptional activator, REDS cells respond to BRD4 inhibition with activation of RFP. We therefore asked whether BRD4 inhibitors directly upregulated other genes. According to RNA-seq of KBM7 cells

treated for 24 hours with 1 μM (*S*)-JQ1, 133 genes were significantly upregulated more than two-fold (**Fig. 1h**). Other cell lines (MOLM-13, KASUMI-1, MV4-11, MOLT-3, MEG-01, K-562) responded similarly, and *e.g.* in MOLM-13 cells 172 genes were upregulated after only 2 hours with (*S*)-JQ1. Remarkably, functional annotation of the (*S*)-JQ1 upregulated gene set revealed a strong cell line-independent enrichment of genes involved in chromatin remodelling (**Supplementary Fig. 2c**), particularly histone genes, corroborating the hypothesis of a global chromatin reorganization following BRD4 inhibition.

We then checked the expression of the genes proximal to the RFP insertion site in WT-KBM7 cells treated with (*S*)-JQ1, in order to see if a chromatin remodelling process was occurring at this locus when inhibiting BRD4. In line with our hypothesis, *RAN* expression decreased while *STX2* mRNA levels increased upon (*S*)-JQ1 treatment (**Fig. 1i**), indicating that BRD4 inhibition not only results in the reduced expression of *RAN*, but also raises the transcription of *STX2*.

Screening for functional BRD4 inhibitors

Although BRD4 is well studied, currently available inhibitors are of limited structural and mechanistic diversity[13,21], and druggable targets upstream or downstream of BRD4 have remained elusive. We aimed to screen for small molecules able to functionally inhibit BRD4. In order to confirm the specificity of our reporter detecting BRD4 inhibition, and not any other epigenetic pertubations, we treated REDS3 with several chromatin-targeted molecules. Within this small panel of compounds, only BET inhibitors were able to activate RFP expression (**Fig. 2a**). With the high specificity of our reporter cell line confirmed, we performed a large live cell imaging screen, testing 89,355 small molecules (**Supplementary Fig. 3a** and **Supplementary Table 1**) for their ability to induce the expression of RFP in REDS3 cells after 24 hours. 0.5 μM (*S*)-JQ1 was used as positive control, as this was the lowest concentration causing full activation of RFP signal (**Supplementary Fig. 3b**) and an excellent Z'-factor[22] (**Supplementary Fig. 3c** and **Supplementary Table 1**). Following hit validation and elimination of autofluorescent compounds, we confirmed 22 compounds as screening hits (**Fig. 2b** and **Supplementary Table 2**). Remarkably, all BRD4 inhibitors contained in the compound library ((*S*)-JQ1[11], PFI1[23], I-BET151[12], I-BET-762[24], Bromosporine, OXT015, RVX208[25], BI-2536[26] and TG-101348[26]) were part of this group, underscoring the validity of the setup. 13 compounds (**1**-**12** and panobinostat) were

new, among which we suspected new BRD4-inhibition scaffolds or even agents with new mechanism of action. RT-PCR for c-MYC revealed that two out of those small molecules were capable of reducing the expression of this oncogene in a dose-dependent manner to a level comparable to (*S*)-JQ1 treatment (**Fig. 2c** and **Supplementary Table 2**). These two compounds were structurally distinct from (*S*)-JQ1 and all the other BRD4 inhibitors. We named them CeMM Epigenetic Compounds CeMMEC1 (**1**) and CeMMEC2 (**2**) (**Fig. 2d**). REDS3 cells treated with CeMMEC1 and CeMMEC2 expressed RFP detected by live cell imaging in a dose-dependent manner (**Supplementary Fig. 3d** and **Supplementary Fig. 3e**). We measured transcriptome-wide effects of CeMMEC1 and CeMMEC2 and compared them to (*S*)-JQ1. While the number of transcripts regulated by CeMMEC1 and CeMMEC2 is lower than for (*S*)-JQ1, there is a significant overlap of the altered gene sets (**Supplementary Fig. 3f**) and a good correlation between the regulated genes (**Supplementary Fig. 3g**). Overall these data indicate that these two compounds belong to new chemical structural classes of functional BRD4 inhibitors. BRD4 inhibitors are mainly developed for applications in oncology, where they reduce the proliferation of certain cancer cells. Therefore, we treated THP1 cells, a human acute monocytic leukemia cell line sensitive to the inhibition of BRD4, with (*S*)-JQ1, CeMMEC1 and CeMMEC2 and analyzed cell cycle profiles and induction of apoptosis after 48 and 72 hours respectively. The cell cycle assay showed a clear and dose-dependent decrease of the number of cells in S-phase, indicative of G1-phase cell cycle arrest with all three compounds (**Fig. 2e**). Moreover, all compounds induced apoptosis, as judged by AnnexinV staining (**Fig. 2f**). In terms of potency, (*S*)-JQ1 showed the strongest effects, followed by CeMMEC2 and CeMMEC1.

Molecular characterization of functional BRD4 inhibitors

To investigate whether CeMMEC1 and CeMMEC2 inhibit BRD4 through direct physical engangement, we tested their ability to compete for binding of the BRD4 bromodomains to an acetylated histone peptide in an Amplified Luminescent Proximity Homogenous Assay (AlphaLISA) immunoassay. CeMMEC1 was neither able to bind the first nor the second bromodomain of BRD4, as no decrease of fluorescence was observed when this compound was added to the assays (**Fig. 3a**). In contrast, CeMMEC2 bound both bromodomains of BRD4, comparably to (*S*)-JQ1 (**Fig. 3a**), when used at 10 μM. Dose response AlphaLISA assays performed with full length

BRD4 (GST-BRD4) showed that CeMMEC2 has an IC_{50} of 0.9 μM compared to 0.2 μM of (*S*)-JQ1 (**Supplementary Fig. 4a**). Similar results were obtained when the individual bromodomains of BRD4 were tested separately (**Supplementary Fig. 4b**).

To comprehensively analyze the binding capability of CeMMEC1 and CeMMEC2 to representative bromodomain proteins, we obtained BromoScan profiles (**Fig. 3b**). Similarly to other BRD4 inhibitors, CeMMEC2 not only bound BRD4 but also all other proteins of the BET family. In contrast, CeMMEC1 only bound BRD4 very weakly, in line with the AlphaLISA data. Surprisingly, this compound showed high affinity for the bromodomains of CREBBP, EP300, BRD9, and the second bromodomain of TAF1 (TAF1 (2)), also confirmed by the sub-micromolar binding constants (**Supplementary Fig. 4c**). Recently CREBBP and EP300 have been described as BRD4 cofactors in regulation of transcriptional control[27], while the interplay between BRD4 and BRD9 or TAF1 has not been reported yet. Since these four bromodomain containing proteins are direct targets of CeMMEC1, we asked whether the loss of one of them could mimic BRD4 inhibition and increase RFP expression in REDS3 cells. We knocked down CREBBP, EP300, BRD9 and TAF1 in REDS3 cells, using two independent shRNA hairpins for each gene. Western Blot was performed to confirm the level of downregulation by each hairpin (**Fig. 3c and Supplementary Fig. 5**). The number of RFP-positive nuclei after knockdown was quantified by live cell imaging. A significant increase of RFP-positive nuclei was observed when downregulating *TAF1*, whereas no increase of RFP-positive nuclei was detected with *BRD9*, *CREBBP* or *EP300* downregulation (**Fig. 3d**). Moreover, as compounds I-CBP112 and CBP30 have been reported as chemical probes for CREBBP and EP300[28–30], we tested them in dose response to see if a further decrease of the activity of these bromodomains could raise the number of RFP-positive cells (**Fig. 3e**). No RFP expression was detected using I-CBP112, the most selective CREBBP/EP300 inhibitor. CBP30 is known to bind BRD4 at high concentrations. Accordingly, doses able to inhibit CREBBP and EP300[29] did not show any effect, while treatment with 10 μM CBP30 resulted in a 1.5 fold increase of RFP-positive cells compared to DMSO treated cells, likely due to BRD4 inhibition.

Several BRD4 inhibitors, including bromosporine and a 3,5-dimethylisoxazole derivative[31], are known to bind TAF1, but currently, there is no specific inhibitor available for this bromodomain containing protein. Given that CeMMEC1 showed high affinity for TAF1 (2), we decided to further characterize this interaction. Isothermal

titration calorimetry (ITC) confirmed that CeMMEC1 binds to TAF1 (2), with a Kd of 1.8 μM (**Fig. 3f**). Similarly, fluorescence resonance energy transfer (FRET) analysis demonstrated that CeMMEC1 displaced a tetra-acetylated H4 peptide with good efficacy from its TAF1 binding site (IC_{50} = 0.9 μM) (**Supplementary Fig. 4d**). It has been shown that some kinase inhibitors can behave as bromodomain inhibitors[26]. In order to asses the specificity of CeMMEC1, we tested binding of the compound to the active sites of 97 representative kinases profile. None of these kinases were inhibited by more than 60% at a concentration of 10 μM CeMMEC1, suggesting bromodomain-specificity of the compound (**Supplementary Fig. 4e**).

We then used molecular docking to generate hypotheses on the binding mode of CeMMEC1 and CeMMEC2. CeMMEC2 is a triazolopyridazine and is predicted to bind to BRD4 similarly to other related triazolophthalazines[32] (**Supplementary Fig. 4f**). The triazole nitrogen is predicted to form a hydrogen bond to a conserved asparagine deep in the peptide binding pocket of BRD4, thereby acting as an acetyllysine mimetic. CeMMEC1 is an N-methylisoquinolinone derivative. Based on the binding of N-methylquinolinone to the bromodomain of ATAD2[33], CeMMEC1 can be modeled into the TAF1 pocket (**Supplementary Fig. 4g**). Its lactam carbonyl is predicted to form a hydrogen bond with N1604 and with Y1561 through a conserved water molecule. In order to test this binding mode, we generated a panel of 28 CeMMEC1 analogs (**13**-**40**; **Supplementary Table 3** and **Supplementary Note**). These compounds we tested for their capability to activate RFP in REDS3 cells, and for binding to the bromodomains of BRD4 (1), CREBBP and TAF1 (2) (**Supplementary Fig. 6a**). Overall, the data are consistent with the molecular model of CeMMeC1 binding, as substitutions on the dihydrobenzodioxin moiety are generally tolerated, and most of the isoquinolinones retain some binding to CREBBP and TAF1. Excitingly, two of the analogs tested, CeMMEC13 (**13**) and CeMMEC14 (**14**), lost all affinity to CREBBP while retaining TAF1 activity. In contrast, CeMMEC15 (**15**) and CeMMEC16 (**16**) can serve as negative controls, as they bound neither of the tested bromodomain proteins nor did they induce RFP expression in REDS3 cells. Both TAF1 specific compounds are structural isomers of the predicted active-site binding isoquinolinone. In CeMMEC13, the isoquinolinone is changed to a quinolinone, whereas in CeMMEC14 the attachment point and orientation of the central amide are altered. We therefore modelled the binding of the specific compounds to TAF1 (2) and BRD4 (1). Both compounds can be

docked into the binding pocket of TAF1 (2), with the quinolinone and isoquinolinone oxo groups forming key hydrogen bonds (**Supplementary Fig. 6b and Supplementary Fig. 6c**). No convincing docking pose were obtained for BRD4 due to clashes with residues L92 and W81.

Finally, as the CeMMEC1-analog CeMMEC13 appeared to be a selective TAF1 inhibitor, we tested for its ability to inhibit binding of BRD4 (1), BRD9, CREBBP, EP300 and TAF1 (2) bromodomains at 10 μM to acetylated substrate (**Supplementary Fig. 6d**). Also among this larger panel, CeMMEC13 showed high selectivity for the TAF1 (2) bromodomain.

TAF1 and BRD4 synergize mediating transcriptional control

Our results showed that the inhibition of TAF1 phenocopies BRD4 inhibition, suggesting a possible functional link between the two bromodomain proteins. Indeed, downregulation of TAF1 in REDS3 cells increased *RFP* expression (**Supplementary Fig. 7a**) and decreased *c-MYC* expression (**Fig. 4a**) to levels comparable to those induced by *BRD4* downregulation. We tested whether these two bromodomain proteins were able to interact directly. 293T cells were transfected with BRD4-FLAG and FLAG pull down performed 48 hours later showed that TAF1 co-immunoprecipitated with FLAG-BRD4 (**Supplementary Fig. 7b**), suggesting a direct interplay of these two bromodomain containing proteins in controlling gene expression.

As our results revealed the role of TAF1 in ensuring BRD4 functionality, we asked whether downregulation of TAF1 could sensitize cells to the inhibition of BRD4. KBM7 cells treated with shRNAs targeting TAF1 or control hairpins were incubated with different concentrations of (*S*)-JQ1 and cell viability was measured after 96 hours. Downregulation of TAF1 decreased cell viability when (*S*)-JQ1 was used at concentrations not able to affect control cells, and further impaired cell number at higher concentrations (**Fig. 4b**). Similarly, we observed the synergism of the new direct BRD4 inhibitor, CeMMEC2, with TAF1 downregulation (**Supplementary Fig. 7c**). Furthermore, the additional inhibition of TAF1 by CeMMEC1 impaired cell viability in TAF1 downregulated cells (**Supplementary Fig. 7d**), indicating that a strong reduction of TAF1 activity alone can be toxic in these cells.

To further provide evidence for a functional relationship between these two bromodomain containing proteins, we simultaneously inhibited TAF1 and BRD4, with

CeMMEC1 or the analogs CeMMEC13 or CeMMEC14 (**Fig. 4c**), which showed comparable induction of RFP expression in REDS3 cells (**Fig. 4d**), and (*S*)-JQ1 respectively. The combination of these compounds in REDS3 cells further boosted RFP expression beyond the increase in single treatments, indicating cooperation between TAF1 and BRD4 on the remodeling of the RFP locus. The same effect was not achieved when using the TAF1-inactive analogs CeMMEC15 and CeMMEC14 (**Fig. 4e and Supplementary Fig. 7e**).

As KBM7 cells are not particularly sensitive to BRD4 inhibitors, we wanted to test whether the synergy between BRD4 inhibitors and TAF1 inhibitors was conserved in BRD4-dependent cancers. Therefore, we tested whether the combined inhibition of TAF1 and BRD4 could arrest the proliferation of THP1 and H23 cells, a lung adenocarcinoma cell line also sensitive to the inhibition of BRD4. We observed that the combination of (*S*)-JQ1 and CeMMEC1 was more efficiently impairing cell viability than the individual treatments (**Fig. 4f, Supplementary Fig. 7f and Supplementary Fig. 7g**). The Bliss independence test[34] confirmed the synergism between these two treatments and showed that the combination between (*S*)-JQ1 and the analog CeMMEC13, was the most effective (**Supplementary Fig. 7h**).

DISCUSSION

Chromatin reporter cell lines have been proposed as models to identify modulators of position effect variegation and chromatin-targeting small molecules[35–38]. In contrast to previous approaches, we developed a strategy to map chromatin reactivation focused on a specific regulator, BRD4. We selected clones that integrated reporters in fully repressed genomic regions and specifically activated the expression of RFP following BRD4 inhibition. The haploid nature of the reporter cell line makes it easily amenable to genetic screens, and its application for the identification of genes in BRD4 functional pathways will provide further insights into BRD4 biology.

With our reporter cell line validated, we first took a chemical genomics approach and identified compounds that functionally antagonize BRD4. In addition to all known BET inhibitors contained in our library, we identified 13 small molecules that have not been linked to BRD4 biology previously. One of these molecules is panobinostat, a clinically approved histone deacetylase (HDAC) inhibitor. Out of more than 40 HDAC-targeting compounds tested, Panobinostat is the sole compound inducing RFP expression in REDS3 cells, indicating a panobinostat-specifc activity. These findings encourage future efforts to fully characterize Panobinostat and all other validated hit compounds regarding their molecular mechanism and protein targets.

We focused our efforts on two compounds, that phenocopy BRD4 inhibitors not only by their ability ot activate RFP reporter expression, but also by repressing *c-MYC*. One of the hit structures, CeMMEC2, turned out to be a novel direct BRD4 inhibitor. Interestingly, several reports exist in the patent literature describing compounds related to CeMMEC2 to inhibit BRD4[39–42]. Moreover, our screen has also yielded compounds that do not strongly bind BRD4 but still activate the reporter cell line. For one of these compounds, CeMMEC1, we have identified TAF1 as the relevant target in our system. TAF1 is the largest component of the TAF subunits contained in the TFIID core, which is part of the pre-initiation complex (PIC) and serves to recognize the TATA box and correctly place RNAPol II for transcription initiation[43–45]. Thereby, TAF1 plays a fundamental role in the assembly of the transcription machinery. Similar to BRD4, TAF1 is essential for the viability of many different cell lines[46,47], and the two proteins interact not only in the regulation of transcription but also physically in co-immunoprecipitation experiments. We show that TAF1 knockdown increases

sensitivity to BRD4 inhibition, and BRD4 inhibitors synergize with CeMMEC1 to impair viability of BRD4-dependent cell lines.

The specific functions of the bromodomains of TAF1 have remained elusive; our results indicate that the second bromodomain of TAF1 is a relevant target in BRD4 driven cancers. CeMMEC1 proves druggability of this domain and suggests further development of isoquinolinones as bromodomain inhibitors[48–50]. More selective analogs such as quinolinone CeMMEC13 open up the avenue to specifically target TAF1 in cancer.

In summary, our results successfully validate the application of haploid epigenetic reporters to identify functional pathways and novel chemical structures regulating chromatin organization and transcriptional control.

ACKNOWLEDGEMENTS

Research in the Kubicek laboratory is supported by the Austrian Federal Ministry of Science, Research and Economy; the National Foundation for Research, Technology, and Development; the Marie Curie Career Integration Grant EPICAL; and the JDRF. This project was supported by SFB grant F4710 of the Austrian Science Fund (FWF). Sara Sdelci acknowledges support by JDRF postdoctoral fellowship 3-PDF-2014-206-A-N "Reprogramming by Loss of Function". JB, CT, OF and SM are funded by the SGC, a registered charity (number 1097737) that receives funds from AbbVie, Bayer, Boehringer Ingelheim, the Canada Foundation for Innovation, the Canadian Institutes for Health Research, Genome Canada, GlaxoSmithKline, Janssen, Lilly Canada, the Novartis Research Foundation, the Ontario Ministry of Economic Development and Innovation, Pfizer, Takeda, and the Wellcome Trust [092809/Z/10/Z].

We thank all the members of the BioOptic Facility of the Research Institute of Molecular Pathology (IMP) and the Institute of Molecular Biotechnology GmbH (IMBA) for their help with cell sorting, Sergei Gresko and Vladimir Ivanov (Enamine Ltd) for compound synthesis, and Kathryn M. Pugh (Target Discovery Institute – TDI; Oxford) for help with analytical chemistry.

COMPETING FINANCIAL INTERESTS

S.S. and S.Ku. have filed a patent application with claims derives from work described in this manuscript.

AUTHOR CONTRIBUTIONS

S.S. and S. Ku. conceived the project, designed experiments, analyzed data and wrote the manuscript with input from all co-authors; S.S. and C-H.L. performed high throughput screens and analyzed data; S.S., C.T., B.K., J.B, O.F. S.Kn. and S.M. performed biochemical binding studies and analyzed data; F.K. generated and analyzed molecular modeling data; P.R., T.P., M.S., C.B., and J.Z. generated and analyzed transcriptomics data; K.V.M.H and G.S-F. performed analytical chemistry and co-wrote the manuscript.

REFERENCES

1. Wang, R., Li, Q., Helfer, C. M., Jiao, J. & You, J. Bromodomain protein Brd4 associated with acetylated chromatin is important for maintenance of higher-order chromatin structure. *J. Biol. Chem.* **287,** 10738–10752 (2012).
2. Dey, A., Chitsaz, F., Abbasi, A., Misteli, T. & Ozato, K. The double bromodomain protein Brd4 binds to acetylated chromatin during interphase and mitosis. *Proc. Natl. Acad. Sci. U. S. A.* **100,** 8758–63 (2003).
3. Filippakopoulos, P. *et al.* Histone recognition and large-scale structural analysis of the human bromodomain family. *Cell* **149,** 214–231 (2012).
4. Floyd, S. R. *et al.* The bromodomain protein Brd4 insulates chromatin from DNA damage signalling. *Nature* **498,** 246–50 (2013).
5. Wu, S. Y. & Chiang, C. M. The double bromodomain-containing chromatin adaptor Brd4 and transcriptional regulation. *J. Biol. Chem.* **282,** 13141–13145 (2007).
6. Zuber, J., Shi, J., Wang, E. & Rappaport, A. RNAi screen identifies Brd4 as a therapeutic target in acute myeloid leukaemia. *Nature* **478,** 524–528 (2011).
7. Wyce, A. *et al.* BET Inhibition Silences Expression of MYCN and BCL2 and Induces Cytotoxicity in Neuroblastoma Tumor Models. *PLoS One* **8,** 1–15 (2013).
8. Yang, Z., He, N. & Zhou, Q. Brd4 recruits P-TEFb to chromosomes at late mitosis to promote G1 gene expression and cell cycle progression. *Mol. Cell. Biol.* **28,** 967–976 (2008).
9. Nagarajan, S. *et al.* Bromodomain Protein BRD4 Is Required for Estrogen Receptor-Dependent Enhancer Activation and Gene Transcription. *Cell Rep.* **8,** 460–469 (2014).
10. Wu, T., Pinto, H. B., Kamikawa, Y. F. & Donohoe, M. E. The BET Family Member BRD4 Interacts with OCT4 and Regulates Pluripotency Gene Expression. *Stem Cell Reports* **4,** 390–403 (2015).
11. Filippakopoulos, P. *et al.* Selective inhibition of BET bromodomains. *Nature* **468,** 1067–1073 (2010).
12. Seal, J. *et al.* Identification of a novel series of BET family bromodomain inhibitors: Binding mode and profile of I-BET151 (GSK1210151A). *Bioorganic Med. Chem. Lett.* **22,** 2968–2972 (2012).
13. Filippakopoulos, P. & Knapp, S. Targeting bromodomains: epigenetic readers of lysine acetylation. *Nat. Rev. Drug Discov.* **13,** 337–56 (2014).
14. Andersson, B. *et al.* KBM-7, a human myeloid leukemia cell line with double Philadelphia chromosomes lacking normal c-ABL and BCR transcripts. *Leukemia* **9,** 2100–8 (1995).
15. Zhu, J. *et al.* Reactivation of Latent HIV-1 by Inhibition of BRD4. *Cell Rep.* **29,** 997–1003 (2012).
16. Banerjee, C. *et al.* BET bromodomain inhibition as a novel strategy for reactivation of HIV-1. *J. Leukoc. Biol.* **92,** 1147–1154 (2012).
17. Schermelleh, L. *et al.* Subdiffraction multicolor imaging of the nuclear periphery with 3D structured illumination microscopy. *Science* **320,** 1332–1336 (2008).

18. Towbin, B. D. *et al.* Step-wise methylation of histone H3K9 positions heterochromatin at the nuclear periphery. *Cell* **150,** 934–947 (2012).

19. The ENCODE Project Consortium. An Integrated Encyclopedia of DNA Elements in the Human Genome. *Nature* **489,** 57–74 (2012).

20. Whyte, W. a *et al.* Master Transcription Factors and Mediator Establish Super-Enhancers at Key Cell Identity Genes. *Cell* **153,** 307–319 (2013).

21. Filippakopoulos, P. *et al.* Benzodiazepines and benzotriazepines as protein interaction inhibitors targeting bromodomains of the BET family. *Bioorganic Med. Chem.* **20,** 1878–1886 (2012).

22. Running, D. M., Ligon, J. B. & Miskioglu, I. A Simple Statistical Parameter for Use in Evaluation and Validation of High Throughput Screening Assays. *J. Biomol. Screen.* **4,** 928–940 (1999).

23. Fish, P. V. *et al.* Identification of a chemical probe for bromo and extra C-terminal bromodomain inhibition through optimization of a fragment-derived hit. *J. Med. Chem.* **55,** 9831–9837 (2012).

24. Mirguet, O. *et al.* Discovery of epigenetic regulator I-BET762: Lead optimization to afford a clinical candidate inhibitor of the bet bromodomains. *J. Med. Chem.* **56,** 7501–7515 (2013).

25. McLure, K. G. *et al.* RVX-208, an inducer of ApoA-I in humans, is a BET bromodomain antagonist. *PLoS One* **8,** (2013).

26. Ciceri, P. *et al.* Dual kinase-bromodomain inhibitors for rationally designed polypharmacology. *Nat. Chem. Biol.* **10,** 305–312 (2014).

27. Roe, J.-S., Mercan, F., Rivera, K., Pappin, D. J. & Vakoc, C. R. BET Bromodomain Inhibition Suppresses the Function of Hematopoietic Transcription Factors in Acute Myeloid Leukemia. *Mol. Cell* **58,** 1028–1039 (2015).

28. Hay, D. a. *et al.* Discovery and optimization of small-molecule ligands for the CBP/p300 bromodomains. *J. Am. Chem. Soc.* **136,** 9308–9319 (2014).

29. Hammitzsch, A. *et al.* CBP30, a selective CBP/p300 bromodomain inhibitor, suppresses human Th17 responses. *Proc. Natl. Acad. Sci.* **112,** (2015).

30. Picaud, S. *et al.* Generation of a selective small molecule inhibitor of the CBP/p300 bromodomain for leukemia therapy. *Cancer Res.* **75,** 5106–5120 (2015).

31. McKeown, M. R. *et al.* Biased multicomponent reactions to develop novel bromodomain inhibitors. *J. Med. Chem.* **57,** 9019–27 (2014).

32. Fedorov, O. *et al.* [1,2,4]Triazolo[4,3-a]phthalazines: Inhibitors of Diverse Bromodomains. *J. Med. Chem.* **57,** 462–476 (2014).

33. Chaikuad, A., Petros, A. M., Fedorov, O., Xu, J. & Knapp, S. Structure-based approaches towards identification of fragments for the low-druggability ATAD2 bromodomain. *Medchemcomm* **5,** 1843–1848 (2014).

34. Bliss, C. I. The toxicity of poisons applied jointly. *Ann. Appl. Biol.* **26,** 585–615 (1939).

35. Johnson, R. L., Huang, W., Jadhav, A., Austin, C. P. & Martinez, E. D. A Quantitative High-Throughput Screen Identifies Potential Epigenetic Modulators of Gene Expression. *Anal. Biochem.* **375,** 237–248 (2008).

36. Best, A. M., Chang, J., Dull, A. B., Beutler, J. A. & Martinez, E. D. Identification of Four Potential Epigenetic Modulators from the NCI Structural Diversity Library Using a Cell-Based Assay. *J. Biomed. Biotechnol.* **2011,** 868095 (2011).

37. Wang, L. *et al.* A small molecule modulates Jumonji histone demethylase activity and selectively inhibits cancer growth. *Nat. Commun.* **4,** 2035 (2013).

38. Tchasovnikarova, I. A. *et al.* Epigenetic silencing by the HUSH complex mediates position-effect variegation in human cells. *Science* **348,** 1481–1485 (2015).

39. BLANK, J. *et al.* Imidazopyrrolidinone derivatives and their use in the treatment of disease. Novartis, WO/2014/191894 (2014).

40. Engelhardt, H. *et al.* Triazolopyridazine. Boehringer Ingelheim, US 2014/0135336 (2014).

41. Blank, J. *et al.* Pyrazolopyrrolidine Derivatives and their Use in the Treatment of Disease. Novartis, WO/2014/191896 (2014).

42. Albrecht, B. K., Harmange, J., Côté, A. & Taylor, A. Bromodomain inhibitors and uses thereof. Constellation pharmaceuticals, Inc., WO/2012/17448 (2012).

43. Lee, D. *et al.* Functional Characterization of Core Promoter Elements : the Downstream Core Element Is Recognized by TAF1. *Mol. Cell. Biol.* **25,** 9674–9686 (2005).

44. Kloet, S. L., Whiting, J. L., Gafken, P., Ranish, J. & Wang, E. H. Phosphorylation-Dependent Regulation of Cyclin D1 and Cyclin A Gene Transcription by TFIID Subunits TAF1 and TAF7. *Mol. Cell. Biol.* **32,** 3358–3369 (2012).

45. Kandiah, E., Trowitzsch, S., Gupta, K., Haffke, M. & Berger, I. More pieces to the puzzle: Recent structural insights into class II transcription initiation. *Curr. Opin. Struct. Biol.* **24,** 91–97 (2014).

46. Wang, T. *et al.* Identification and characterization of essential genes in the human genome. *Science* **350,** 1096–1101 (2015).

47. Blomen, V. A. *et al.* Gene essentiality and synthetic lethality in haploid human cells. *Science* **350,** 1092-96 (2015).

48. Arrowsmith, C. H. *et al.* The promise and peril of chemical probes. *Nat. Chem. Biol.* **11,** 536–541 (2015).

49. Workman, P. & Collins, I. Probing the Probes: Fitness Factors For Small Molecule Tools. *Chem. Biol.* **17,** 561–577 (2010).

50. Frye, S. V. The art of the chemical probe. *Nat Chem Biol* **6,** 159–161 (2010).

FIGURE LEGENDS

Figure 1 | Generation of a reporter cell line for the inhibition of BRD4

(**a**) Graphic representation of the experimental approach. (**b**) Sorting panels representing the WT-KBM7 population (not infected), the infected and sorted population (red square: RFP-positive and sorted cells), and the double sorted population (black square: RFP negative and double sorted cells). (**c**) Representative FACS panels of REDS3 cells treated with 0.5 μM (*R*)-JQ1, 0.5 μM (*S*)-JQ1 or control DMSO for 18 hours. At least three biological replicates were done for each experimental condition. (**d**) Quantification of RFP-positive cells by FACS, following knock-down of the indicated bromodomain proteins in REDS3 cells; three biological replicates were done for each experimental condition and at least 30,000 cells were analyzed each time (mean±STD). (**e**) Representative images of REDS3 cells with sh2-mediated knock-down of BRD3 or BRD4; scale bar 100 μm. (**f**) Representative pictures of the FISH assay in REDS3 cells, stained for the RFP insertion (FISH probe, purple) and nucleus (blue, perimeter marked by yellow dashed lines). Scale bar 10 μm. (**g**) Categorization of cells by the distance between the RFP FISH probe and the nuclear membrane, indicated as near (< 2 μm) and far (> 2 μm); duplicates were performed and at least 80 cells were counted for each experimental condition (mean±STD). (**h**) Volcano plot representing gene expression changes in KBM7 cells upon treatment with 1 μM (*S*)-JQ1 for 24 hours, compared to DMSO treatment (RNAseq data analysis; grey dots, not significant (*q*value > 0.05) / red dots, significant (*q*value < 0.05)). (**i**) RT-PCR showing *STX2* and *RAN* fold change upon treatment with 1 μM (*S*)-JQ1 for 24 hours in KBM7 cells. Values are normalized to actin expression and DMSO treated cells. Three biological replicates were done for each condition (mean±STD).

Figure 2 | Screening for functional BRD4 inhibitors

(**a**) Heat map showing the increase of RFP-positive nuclei in REDS3 clone treated with the compounds shown at 1, 5 and 10 μM for 24 hours (triplicates, % of control, DMSO is used as negative control and (*S*)-JQ1 20 μM as positive control). (**b**) Scatter plot representing the hit distribution from the last part of the validation screen. The variable RED was calculated as the product of the number of red cells multiplied by the median

red intensity. Autofluorescent compounds increase RED in WT-KBM7 cells, whereas hit compounds act only in REDS3 cells. (**c**) Relative c-MYC expression in WT-KBM7 treated with the selected compounds, assessed by RT-PCR. 1, 10 and 20 μM of each compound were used to treat cells for 24 hours; DMSO was used as negative control and (*S*)-JQ1 as positive control. Three biological replicates were performed (mean±STD). (**d**) Chemical structures of (*S*)-JQ1, CeMMEC1 (**1**) and CeMMEC2 (**2**). (**e**) Quantification of cells in S-phase by staining the nuclei with PI and analyzing DNA content by FACS. THP1 cells were treated with DMSO or the indicated concentrations of (*S*)-JQ1, CeMMEC1 or CeMMEC2 for 48 hours. Three different biological replicates were performed and 30,000 cells were analysed each time (mean±STD). (**f**) Quantification of AnnexinV positive cells from immunofluorescence images. Cells were treated with DMSO or the indicated concentrations of (*S*)-JQ1, CeMMEC1 or CeMMEC2 for 72 hours. At least 3 biological replicates were performed and more than 1,500 cells were quantified for each point (mean±STD).

Figure 3 | Molecular and cellular characterization of CeMMEC1 and CeMMEC2

(**a**) AlphaLISA assays for the first (black columns, BD1) and the second (grey columns, BD2) bromodomains of BRD4, incubated with CeMMEC1 (**1**) and CeMMEC2 (**2**). (*S*)-JQ1 and RVX-208 were used as positive controls. The assay was done in duplicate (mean±STD); all compounds were used at 10 μM. (**b**) BromoScan profile for CeMMEC1 (red bubbles) and CeMMEC2 (pink bubbles) (10uM). Bubbles indicate the percentage of inhibition of the binding of the analyzed bromodomains to an acetylated substrate. (**c**) Representative Western Blots showing knock down levels of the indicated bromodomain downregulated using two different shRNAs (shRNA C = control_sh; shRNA 1 = hairpin nr.1; shRNA 2 = hairpin nr.2) (**d**) Quantification of RFP-positive REDS3 cells upon downregulation of the indicated bromodomains from live cell imaging pictures. Three replicates were perfromed and more than 1,500 cells were quantified for each point (% of control, negative control is control_sh treated with DMSO, positive control is control_sh treated with (*S*)-JQ1; mean±STD). (**e**) Fold change of RFP-positive cell numbers quantified from live cell imaging pictures of REDS3 clone treated with the indicated compounds at the displayed concentrations for 24 hours (DMSO normalized; duplicates, at least 1500 cells were quantified in each

replicate). (**f**) Isothermal Titration Calorimetry (ITC) results for CeMMEC1 with the second bromodomain of TAF1.

Figure 4 | TAF1 synergizes with BRD4 to mediate transcriptional control

(**a**) Fold change of c-MYC expression assessed by RT-PCR in WT-KBM7 with knockdown of TAF1 or BRD4 (compared to control cells); three biological replicates were performed (mean±STD). (**b**) CellTiterGlo assay of control and TAF1 downregulated WT-KBM7 treated with the indicated concentrations of (*S*)-JQ1 (each point performed at least in triplicate, an equal amount of DMSO was added as control). (**c**) Chemical structures of the indicated CeMMEC1 analogs **13**-**16**. (**d**) Fold-change of RFP-positive cell numbers quantified from live cell imaging pictures of REDS3 clone treated with the indicated compounds at the displayed concentrations for 24 hours (DMSO normalized; duplicates, at least 1500 cells were quantified in each replicate). (**e**) Matrix displaying fold change of REDS3 RFP-positive cells treated with the indicated concentrations of (*S*)-JQ1, CeMMEC1 (**1**), analog CEMMEC13 (**13**) and analog CeMMEC15 (**15**) alone or in combination (each point at least in triplicate). (**f**) Matrix displaying cell viability reduction of H23 cells treated with the indicated concentrations of (*S*)-JQ1, CeMMEC1, analog CEMMEC13 and analog CeMMEC15 alone or in combination (each point done at least in duplicate, an equal amount of DMSO was added as control). Statistics (Student's t-test, two tails): * indicates 0.05 < *p*value < 0.01; ** indicates 0.01 < *p*value < 0.001; *** indicates *p*value < 0.001.

ONLINE METHODS

Cell culture and transfection

The human chronic myelogenous leukemia cell line KBM7 was cultured in Iscove's Modified Dulbecco's Medium (IMDM, Gibco), supplemented with 10% Fetal Bovine Serum (FBS; Gibco) and 100 units/ml streptomycin and penicillin (both from Gibco). The human embryonic kidney cell line HEK293T was cultured in Dulbecco's Modified Eagles Medium (DMEM, Gibco) supplemented with 10% FBS and 100 units/ml streptomycin and penicillin. The peripheral blood human acute monocytic leukemia cell line THP1 and the adenocarcinoma (non small lung cancer) cell lines H23 were cultured in RPMI-1640 (Roswell Park Memorial Institute, Gibco) supplemented with 10% FBS and 100 units/ml streptomycin and penicillin. All the mentioned cell lines were incubated in 5% CO2 atmosphere at 37°C.

HEK293T cells were transfected with Lipofectamine 2000 (Invitrogen) according to the manufacturer's instructions.

Used plasmids were:

LZRS-RFP-ires-ZEO (a gift from Sebastian Nijman).

pFlag-CMV2-Brd4 (a gift from Eric Verdin, Addgene plasmid # 22304).

Live cell imaging and picture quantification

Cells were seeded on clear flat bottom 96-well or 384-well plates (Corning) and treated with the indicated compounds for the specified conditions. Live cell imaging pictures were taken with the Operetta High Content Screening System (PerkinElmer), 20X objective and non-confocal mode.

RFP quantification was done using the Harmony software (PerkinElmer) for nuclei detection and analysis, adapted for the nucleus diameter range of the specific cell line used (*e.g.* KBM7 nucleus diameter 13 μM). Only RFP-positive nuclei were detected and counted.

Apoptotic cells were detected using the Annexin V-FITC Apoptosis detection kit (Abcam) according to the manufacturer's instruction. Apoptosis quantification was performed with the Harmony software (PerkinElmer) for nuclei and cytoplasm detection

and analysis, adapted for the nucleus diameter range and cell shape of the specific cell line used.

Western Blot

Proteins were separated on polyacrylamide gels with SDS running buffer (50 mM Tris, 380 mM Glycine, 7 mM SDS) and transferred to nitrocellulose blotting membranes. All membranes were blocked with blocking buffer (5% (m/v) milk powder (BioRad) in TBST (Tris-Buffered Saline with Tween: 50 mM Tris (tris (hydroxymethyl)aminomethane), 150 mM NaCl, 0,05% (v/v) Tween 20, adjusted to pH 7.6)). Proteins were probed with antibodies against BRD4 (ab128874, 1:1000, Abcam), Actin (ab16039, 1:1000, Abcam), c-MYC (ab32072, 1:1000, Abcam), Flag (F1804, 1:1000, Sigma), BRD9 (ab49313, 1:1000, Abcam) and Taf1 (sc-735, 1:1000, Santa Cruz), detected by HRP (horseradish peroxidase) conjugated donkey anti-rabbit IgG antibody (ab16284, 1:5000, Abcam) or donkey anti-mouse IgG antibody (Pierce) and visualized with the Pierce ECL Western Blotting substrate (Amersham), according to the provided protocol.

RNA extraction PCR and QPCR

RNA extraction was performed with TRIzol Reagent (Life Technologies) according to the manufacturer's protocol and Reverse Transcription (RT) was performed using the High Capacity cDNA Reverse Transcription Kit (Applied Biosystems) following the standard protocol.

Standard PCR was performed using Pfu DNA Polymerase (Fermenta) according to the standard conditions.

Standard PCR primers used:

WT-KBM7 genome (Sigma; forward 5'-CAGTTCCGCTACACGTGCTG, reverse 5'-CGTGGACCCTTAAAGAGAAGGT)

REDS3 genome (Sigma; forward 5'- CAGTTCCGCTACACGTGCTG, reverse 5'-GCGCATGAACTCCTTGATGAC)

Insulin_promoter (Sigma; forward 5'-CTCTCCTTGAGATGTTAATGTGGCT, reverse 5'-CACACGGAAGATGAGGTCCGAGTGG)

QPCR was performed using the Power SYBR Green Master mix (Invitrogen) as described in the manufacture's protocol.

QPCR primers used:

BRD4 (Sigma; forward 5'-CAGGAGGGTTGTACTTATAGCA, reverse 5'-CTACTGTGACATCATCAAGCAC).

c-MYC (Sigma; forward 5'-GAAGGTGATCCAGACTCTFACCT, reverse 5'-CTTCTCTCCGTCCTCGGATTCT).

Actin (Sigma; forward 5'-ATGATGATATCGCCGCGCTC, reverse 5'-CCACCATCACGCCCTGG).

BRD3 (Sigma; forward 5'-AAGAAGAAGGACAAGGAGAAGG, reverse 5'-CTTCTTGGCAGGAGCCTTCT).

TAF1 (Sigma; forward 5'-TGCCCAGGAGATTGTGAACG, reverse 5'-GGCTTAGCCTGAGGCGTG).

CREBP (Sigma; forward 5'-AGCAGCAGCTGGTTCTACTG, reverse 5'-CACAATGGGCAACTTGGCAG).

EP300 (Sigma; forward 5'-GCAGTGTGCCAAACCAGATG, reverse 5'-CATAGCCCATAGGCGGGTTG).

STX2 (Sigma; forward 5'-GGCAAGAAGGAAATTGATGTTCA, reverse 5'-AGACGTTCGGTTGTGCTTCT).

RAN (Sigma; forward 5'-GAGAAGAACCACCTTGGGTGT, reverse 5'-TCCACCGAATTTCTCCTGGC).

RFP (Sigma; forward 5'-GGGAGCGCGTGATGAACTTC, reverse 5'-GGAAGTTCACGCCGATGAAC).

Real-time amplification results were normalized to the endogenous housekeeping genes Actin or GAPDH. The relative quantities were calculated using the comparative CT (Cycle Threshold) Method (ΔΔCT Method).

Cell cycle assay and cell sorting

For cell cycle analysis, cells were fixed with 70% ethanol for 24 hours, washed with PBS/0.1%-Tween and incubated with RNase for 20 minutes. Nuclei were stained with 5 ug/ml PI (propidium iodide, Sigma) for 10 minutes prior to FACS analysis (BD FACSCalibur Flow Cytometer).

RFP-positive/negative cell sorting was performed using the FACSAria (BD Biosciences) sorter. Gates for positive or negative RFP populations were done using the appropriate RFP-positive or negative controls. RFP-positive cells (1%, very positive population) were sorted in presence of (*S*)-JQ1 0.5 µM 48 hours after infection. The negative population was sorted in absence of (*S*)-JQ1 72 hours after the first sorting (0.7%, negative, double-sorted single clones). RFP negative double-sorted clones were grown and treated with (*S*)-JQ1 0.5 µM several times, in order to verify their ability to express RFP only upon treatment.

FISH assay

The RFP specific probe (RFPprobe) was PCR performed using RFP specific primers (Sigma; forward 5'-CGGTTAAAGGTGCCGTCTCG, reverse 5'-AGGCTTCCCAGGTCACGATG) and labeled using dig-dUTP (DIG Nick Translation Mix, Roche).

Briefly, before hybridization, slides were fixed with 3% paraformaldehyde (Merck) in PBS for 10 min, permeabilized with 0.5% Triton (Sigma) in PBS for 5 min and then immediately passed through an ethanol series (70%, 85% and 100%). The denaturation was performed in 50% formamide (Sigma) in 2XSSC buffer (Saline Sodium Citrate buffer: 0.3 M NaCl, 30 mM sodium citrate) simultaneously on nuclei and probes for 30 min at 80°C. Hybridization was done overnight in a dark humidity chamber at 37°C. The slides were washed three times in 50% formamide/2XSSC buffer and another three times with 50% 2XSSC buffer (both at room temperature), incubated with Anti-Digoxigenin-Fluorescein (Fab fragments, Roche) for 1 hour at room temperature and detected with AlexaFluor488 IgG Fraction Monoclonal Mouse Anti-Fluorescein (Jackson Laboratory). Finally, nuclei were counterstained with 4',6-diamidino-2-phebyl-indole (DAPI, Sigma). Images were taken using a Leica DMI6000b inverted confocal system and a 63X 1.30 ACS Apo lens, and edited using Leica LAS AF software (Leica Microsystems) and Fiji (ImageJ).

Protein Expression of GST-tagged BRD4

GST-BRD4 was extracted and purified from BL21 (DE3) *E.coli* cells (New England BioLabs) and heat shock transformed with p5068 pGEX-6P-1 (full length BRD4 with GST-tag; a gift from Peter Howley (Addgene)). Transformed cells were inoculated into a LB agar plate with ampicillin 100 mg/ml. One colony was selected and grown in LB broth (ampicillin 100 mg/ml) in a shaker (250*g*) at 37°C until an OD (optical density) value of 0.8 at 600 nm was reached. Isopropyl-β-D-thiogalactopyranoside (IPTG; Sigma) was added to a final concentration of 0.3 mM, cultures were further grown for 3 hours at 37°C. Cells were harvested by centrifugation (6000*g* for 15 min at 4°C) and resuspended in cold lysis buffer (20 mM Tris-HCl pH 7.5, 0.5 M NaCl, 5 mM EDTA, 1% Igepal) containing 2.5 mg/ml Lysozyme (Fluka), 0.1 mg/ml DNase I (Roche), 5 mM β-mercaptoethanol and an appropriate amount of protease inhibitor cocktail (Roche). Cells were disrupted by gentle sonication (2 cycles, 10s) on ice and centrifuged (9000*g* for 20 min at 4°C). BRD4 proteins carrying the GST-tag were purified under native conditions using Glutathione Sepharose 4B beads (GE Healthcare). The GST-tagged proteins were eluted with elution buffer (10 mM Glutathione, 50 mM Tris, pH 8.0, plus appropriate amount of protease inhibitor cocktail). The purity of the protein preparations was assessed by SDS-PAGE in 10% polyacrylamide gel, under reducing conditions.

AlphaLISA Assay

The Amplified Luminescent Proximity Homogenous Assay (AlphaLISA©)[51] is the homogenous and *chemiluminescence*-based method, used to explore the direct interaction of the identified small molecules with BRD4 and therefore, measure the IC_{50} values of the direct BRD4 inhibitors.

Briefly, in this assay, the biotinylated histone peptide substrate is captured by streptavidin-coupled donor beads. The GST-tagged bromodomain is recognized and bound by an anti-GST antibody conjugated with an acceptor bead. In absence of an inhibitor, the bromodomain binds to histone peptide substrate. The excitation (680 nm wavelength) of a donor bead provokes the release of a singlet oxygen molecule ($^1O_2$) that triggers a cascade of energy transfer in the acceptor bead, resulting in a sharp peak of light emission at 615 nm. The event of a signal (alpha count) can only take place when the interaction partners are in proximity (< 200 nm). The presence of a

compound that blocks the histone-docking site (inhibitor) results in the dropping of emission.

The AlphaLISA was performed for both bromodomains of BRD4 using the BRD4 (BD1) Inhibitor Screening Kit (BPS Bioscience) and BRD4 (BD2) Inhibitor Screening Kit (BPS Bioscience) following the manufacturer's protocol. For the GST full length BRD4 purified from BL21 cells, a mixture of acetylated substrates from the BD1 and BD2 Inhibitor Screening Kit reported above was used.

Compounds were tested at a final assay concentration of 10 μM in duplicates. To determine IC_{50} values, two-fold serial dilutions (12 points; 50 μM to 0.02 μM) of test inhibitors were prepared. Reaction was initiated by adding one of the two bromodomains (BD1 or BD2) or the GST full length BRD4. After 30 minutes, GSH (Glutathione) Acceptor beads (PerkinElmer) were added and after another incubation time of 30 minutes, Streptavidin-conjugated donor beads (PerkinElmer) were added. Alpha counts were read by EnVision 2104 Multilabel Reader (PerkinElmer).

Compound screening

REDS3 cells were treated with the compound library (89,355 diverse compounds). The increase of RFP fluorescence, detected with the Operetta High Content Screening System (PerkinElmer), 20X objective and non-confocal mode, was used as read-out.

Briefly, the screening was divided in three parts called respectively 1) primary screening, 2) follow up and 3) validation. During the primary screening REDS3 cells were treated with 10 μM of every compound, and live cell imaging pictures were taken in order to assess their ability to induce RFP expression 24 hours later. From this primary screening 1,286 small molecules were selected as hits and re-screened in the follow up part, in which REDS3 and WT-KBM7 were treated in 3-point dose response in order to exclude autofluorescent or toxic compounds. 80 small molecules were selected as hits and used to treat WT-KBM7 and REDS3 in 8-point dose (2 fold dilution, starting from 100 μM) response and 3-point time course (24/48/72 hours) in order to carefully select the best true hits (time- and dose-dependent RFP expression/no autofluorescence). UPLC-MS analysis was done to confirm purity and the correct mass of the small molecules selected; finally, 22 small molecules fulfilled the criteria as screening hits.

Compound synthesis and characterization

Commercial compounds were obtained from ChemDiv Inc, Enamine Ltd., Interbioscreen, LC Laboratories, Medchemexpress Europe, Chemietek, Tocris Bioscience, Selleck Chemicals. CeMMEC 1 analogs were synthesized by Enamine Ltd. All compounds were quality controlled by LC-MS, requiring a minimum purity of 90%. Detailed information including catalogue numbers for commercial compounds, synthetic methods for CeMMEC1 analogs and analytical data on all compounds are provided as **Supplementary Note**.

RNA-sequencing

The amount of total RNA was quantified using Qubit 2.0 Fluorometric Quantitation system (Life Technologies) and the RNA integrity number (RIN) was determined using Experion Automated Electrophoresis System (Bio-Rad). RNA-seq libraries were prepared with TruSeq Stranded mRNA LT sample preparation kit (Illumina) using Sciclone and Zephyr liquid handling robotics (PerkinElmer). Library amount was quantified using Qubit 2.0 Fluorometric Quantitation system (Life Technologies) and the size distribution was assessed using Experion Automated Electrophoresis System (Bio-Rad). For sequencing libraries were pooled and sequenced on Illumina HiSeq 2000 using 50 bp single-read. Reads were aligned with tophat (v2.0.4) with the --no-novel-juncs --no-novel-indels options[52].Gene expression was calculated as Reads Per Kb per Millions of reads (RPKMs) using RPKM_count.py from RSeQC package[53] and the NCBI RNA reference sequences collection (RefSeq) downloaded from UCSC[54]. The enrichment calculation was done by Gene Set Enrichment Analysis[55,56].The amount of total RNA was quantified using Qubit 2.0 Fluorometric Quantitation system (Life Technologies) and the RNA integrity number (RIN) was determined using Experion Automated Electrophoresis System (Bio-Rad). RNA-seq libraries were prepared with TruSeq Stranded mRNA LT sample preparation kit (Illumina) using Sciclone and Zephyr liquid handling robotics (PerkinElmer). Library amount was quantified using Qubit 2.0 Fluorometric Quantitation system (Life Technologies) and the size distribution was assessed using Experion Automated Electrophoresis System (Bio-Rad). For sequencing libraries were pooled and sequenced on Illumina HiSeq 2000 using 50 bp single-read. Reads were aligned with tophat (v2.0.4) with the --no-novel-juncs --no-novel-indels options[52].Gene expression was calculated as Reads Per Kb per Millions of reads (RPKMs) using RPKM_count.py from RSeQC package[53] and

the NCBI RNA reference sequences collection (RefSeq) downloaded from UCSC[54]. The enrichment calculation was done by Gene Set Enrichment Analysis[55–58].

TAF1 binding assay

TAF1 binding assays were conducted using the EPIgeneous™ Binding Domain kit B (Cisbio Bioassays) according to manufacturer's instructions. Binding was determined by the displacement of an acetylated biotin-peptide from a GST tagged TAF1 protein using HTRF with a Eu3+ conjugated GST antibody donor and streptavidin conjugated acceptor. Compounds were dispensed into assay plates, ProxiPlate-384 Plus (Perkin Elmer) using an Echo 525 Liquid Handler (Labcyte). Binding assays were conducted in a final volume of 20 µl with 5 nM TAF1-GST, 50 nM peptide (SGRGK (ac)GGK (ac)GLGK (ac)GGAK (ac)RHRK (biotin)-acid), 6.25 nM Streptavidin-XL665, 1:200 Anti-GST-Eu3+ cryptate and 0.1 % DMSO. Assay reagents were dispensed into plates using a Multidrop combi (Thermo Scientific) and incubated at room temperature for 3 hours. Fluorescence was measured using a PHERAstar microplate reader (BMG) using the HTRF module with dual emission protocol (A = ex. 320 nm em. 665 nm, B = ex. 320 nm em. 620 nm). Raw data were processed to give an HTRF ratio (channel A/B *10000), which was used to generate IC_{50} curves.

Protein expression and purification of TAF1 second bromodomain

TAF1 second bromodomain (Uniprot P21675, residues 1501-1634) was cloned into a pET28 derived expression vector, pNIC28-Bsa4 using ligation independent cloning. Colonies transformed in competent *E. coli* BL21 (DE3)-R3-pRARE2 cells (phage-resistant derivative of BL21 (DE3) strain), with a pRARE plasmid encoding rare codon tRNAs were grown overnight at 37ºC in 10 ml of Terrific broth medium (Sigma) with 50 µg/ml kanamycin and 34 µg/ml chloramphenicol. Cells were grown at 37ºC in TB from overnight cultures until A600 reached between 0.8-1.1, then the media was cooled and 0.2 mM Isopropyl-β-D-thiogalactopyranoside (IPTG) was added to induce the protein expression at 18ºC for 16 hours. The bacteria were harvested by centrifugation (JLA 8,100 rotor Beckman Coulter Avanti J-20 XP centrifuge) and were frozen at -20ºC. Cell expressing 6xHis tagged TAF1 second bromodomain were re-suspended in lysis buffer (20 mM Hepes pH 7.5, 500 mM NaCl, 10 mM Imidazole, 5% glycerol and 0.2 mM TCEP (Tris (2-carboxyethyl)phosphine hydrochloride) in the presence of protease inhibitors cocktail (1 µl/ml) and lysed using an EmulsiFlex-C5 high pressure

homogenizer (Avestin-Mannheim, Germany) at 4ºC. The lysate was cleared by centrifugation (14,000 x g for 1 hour at 4ºC). After centrifugation, the supernatant was loaded onto the nickel column and eluted in an imidazole linear gradient. The eluted protein was collected and treated overnight with TEV protease at 4ºC to remove the N terminal tag. Digested protein was loaded onto a nickel column again to remove the non-cleaved protein and the hexa-histidine TEV used. The flow through containing the untagged protein was collected and further purified through a size exclusion chromatography in 20 mM Hepes pH 7.5, 500 mM NaCl, 5% glycerol and 0.2 mM TCEP (HiLoad 16/60 Superdex 75 GE Healthcare Life Sciences). Similarly, GST-tagged TAF1 second bromodomain was purified using a 5 μλ Glutathione Sepharose Fast Flow column with elution buffer of 50 mM Tris pH8, 10 mM reduced glutathione. Gel filtration (HiLoad 16/60 Superdex 200) chromatography was performed as the final purification step. The correct mass and purity for both constructs were confirmed by an Agilent 1100 Series LC/MSD TOF (Agilent Technologies Inc. – Palo Alto, CA).

Isothermal Titration Calorimetry

Calorimetric experiments were performed on a VP-ITC micro-calorimeter (MicroCal™, LLC Northampton, MA). TAF1 (2) was buffer exchanged by dialysis into buffer 20 mM Hepes pH 7.5, 150 mM NaCl, and 0.5 mM TCEP. All measurements were carried out at 293.15 K while stirring at 286 rpm. The micro syringe was loaded with a protein solution of 295 μM, the compound solution was prepared at 25 μM and 2 ml for the cell. All injections were performed using an initial injection of 2 μl followed by 34 injections of 8 μl with a duration of 16 seconds per injection and a spacing of 240 seconds between injection. The data were analysed with the MicroCal ORIGIN software package employing a single binding site model. The first data point was excluded from the analysis. Thermodynamic parameters were calculated ($\Delta G = \Delta H - T\Delta S = -RT\ln K_B$ where ΔG, ΔH and ΔS are the changes in free energy, enthalpy and entropy of binding, respectively).

Molecular Modeling

The crystal structures of the second bromodomain of TAF1, of ATAD2 and of BRD4 were downloaded from the RCSB protein data bank (pdb:4qst, pdb:3uv4 and pdb:3mxf). The structures were corrected, protonated and energy minimized using the LigX workflow of the molecular modeling software MOE (Molecular Operating

Environment (MOE), 2014; Chemical Computing Group Inc., 1010 Sherbooke St. West, Suite #910, Montreal, QC, Canada, H3A 2R7). The hit compounds were prepared with the washing tool in MOE.

For binding pose prediction, the template-based docking protocol of MOE was used. CeMMEC1 (**1**) was docked into the crystal structure of the second bromodomain of TAF1 (pdb:3uv4)[3] using the atom positions of 1-methylquinolin 2-one bound to the bromodomain of ATAD2 (pdb:4qst)[33] as template for pose prediction. Similarly, CeMMEC2 (**2**) was docked into a crystal structure of JQ1 bound to BRD4 (pdb:3mxf)[11], with the triazole ring serving as pose prediction template.

METHODS-ONLY REFERENCES

51. Bielefeld-Sevigny, M. AlphaLISA immunoassay platform- the 'no-wash' high-throughput alternative to ELISA. *Assay Drug Dev. Technol.* **7,** 90–92 (2009).

52. Kim, D. *et al.* TopHat2: accurate alignment of transcriptomes in the presence of insertions, deletions and gene fusions. *Genome Biol.* **14,** R36 (2013).

53. Wang, L., Wang, S. & Li, W. RSeQC: Quality control of RNA-seq experiments. *Bioinformatics* **28,** 2184–2185 (2012).

54. Kent, W. J. *et al.* The Human Genome Browser at UCSC. *Genome Res.* **12,** 996–1006 (2002).

55. Subramanian, A. *et al.* Gene set enrichment analysis: a knowledge-based approach for interpreting genome-wide expression profiles. *Proc. Natl. Acad. Sci. U. S. A.* **102,** 15545–50 (2005).

56. Mootha, V. K. *et al.* Integrated analysis of protein composition, tissue diversity, and gene regulation in mouse mitochondria. *Cell* **115,** 629–640 (2003).

57. Huang, D. W., Sherman, B. T. & Lempicki, R. a. Systematic and integrative analysis of large gene lists using DAVID bioinformatics resources. *Nat. Protoc.* **4,** 44–57 (2009).

58. Huang, D. W., Sherman, B. T. & Lempicki, R. a. Bioinformatics enrichment tools: Paths toward the comprehensive functional analysis of large gene lists. *Nucleic Acids Res.* **37,** 1–13 (2009).

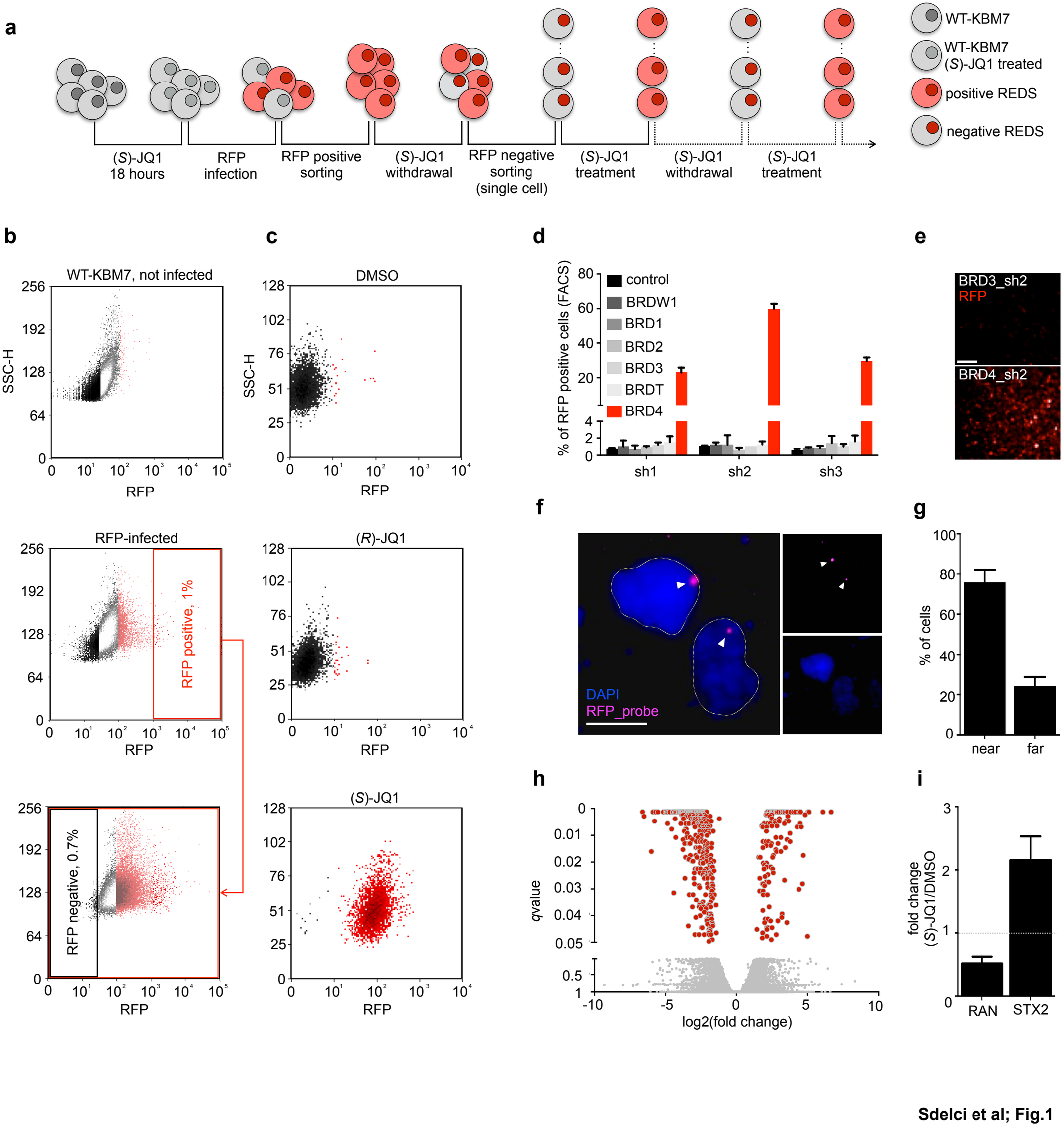

Sdelci et al; Fig.1

a

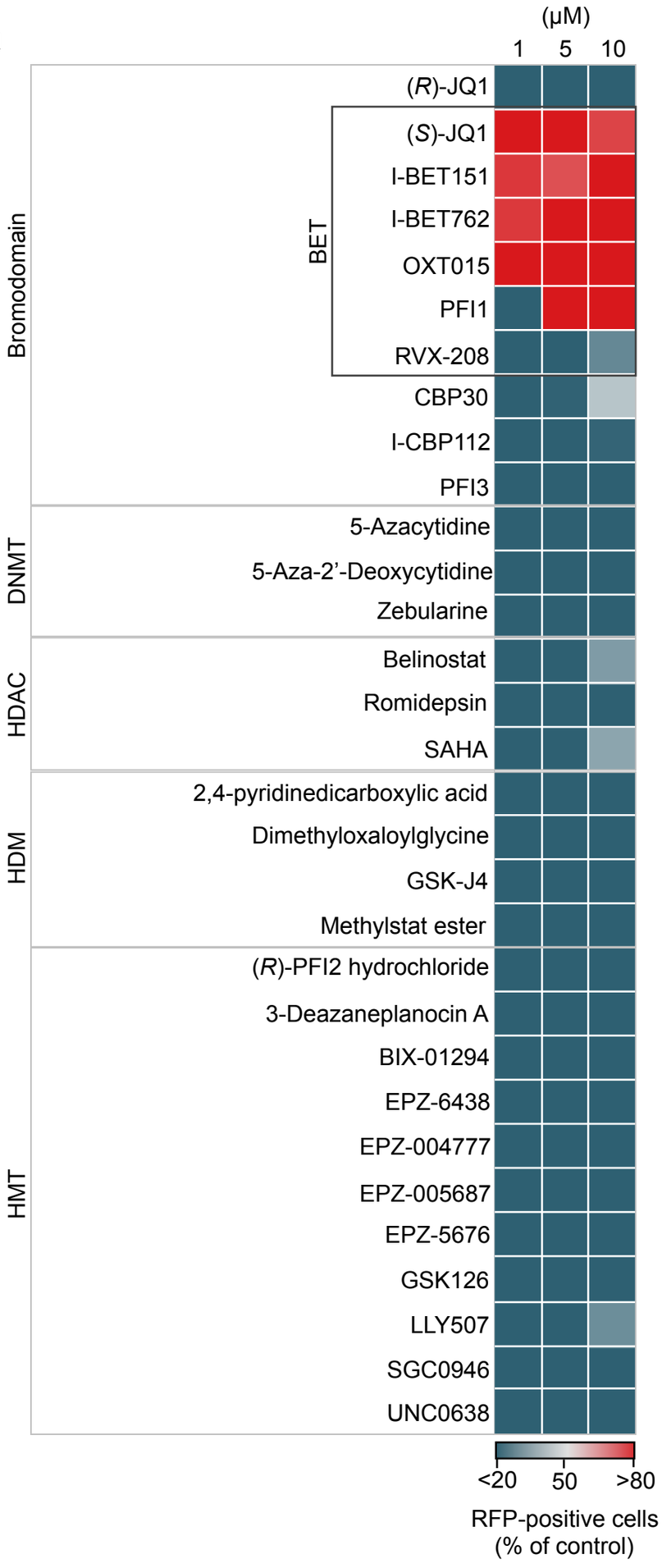

b

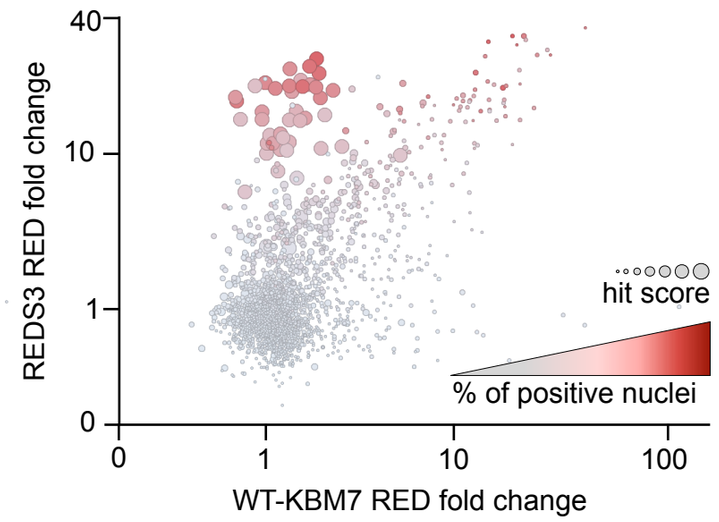

c

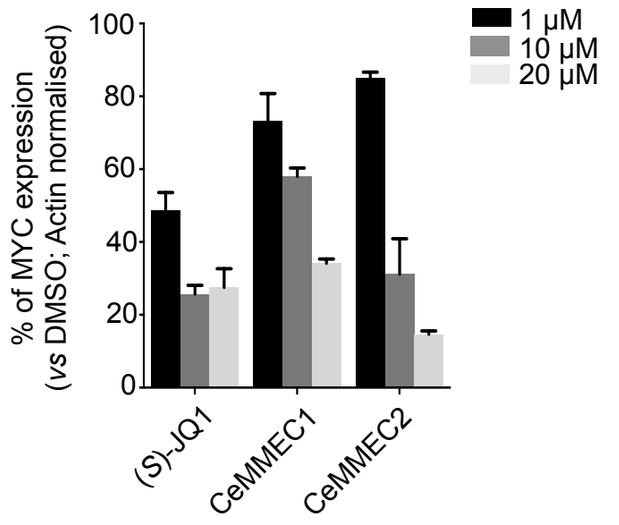

d

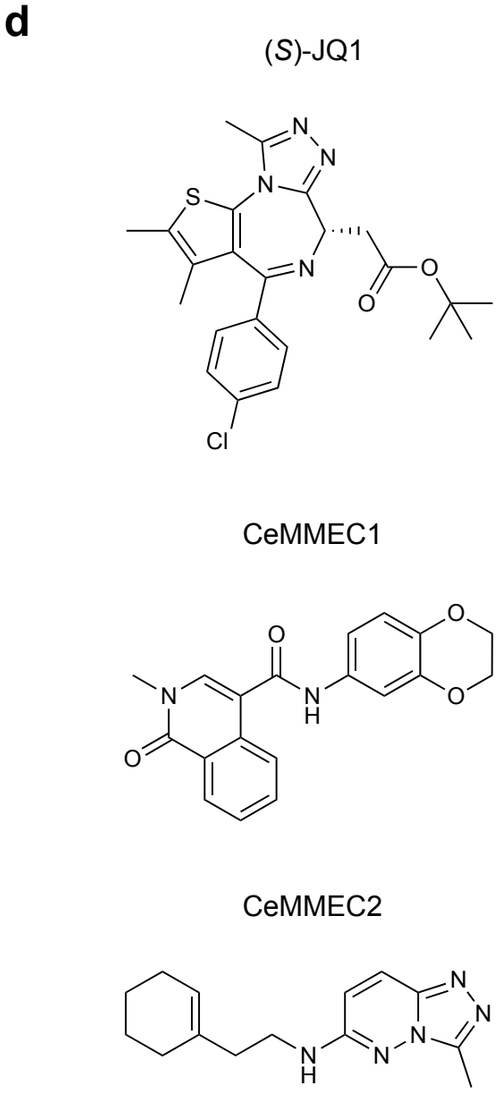

e

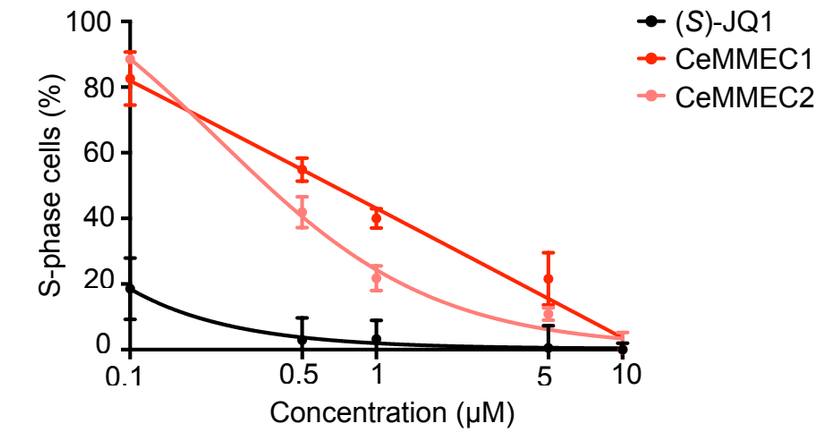

f

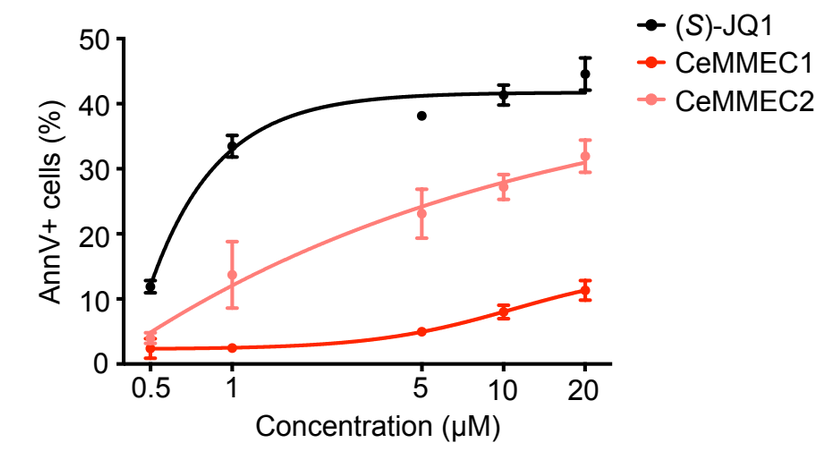

Sdelci et al; Fig.2

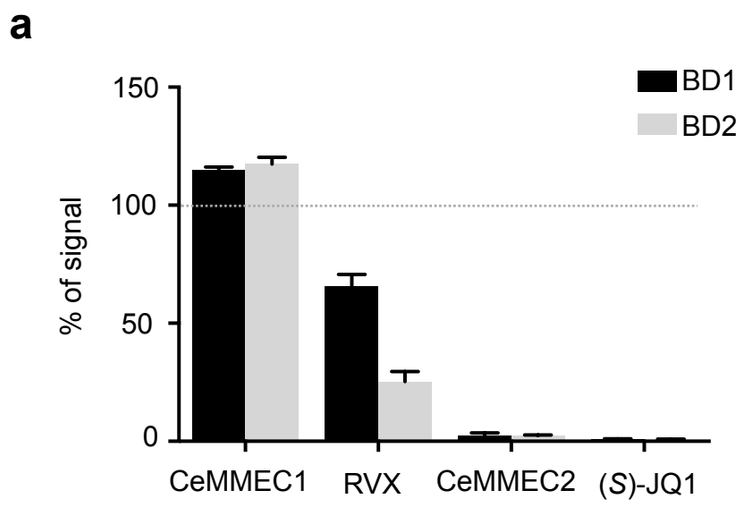

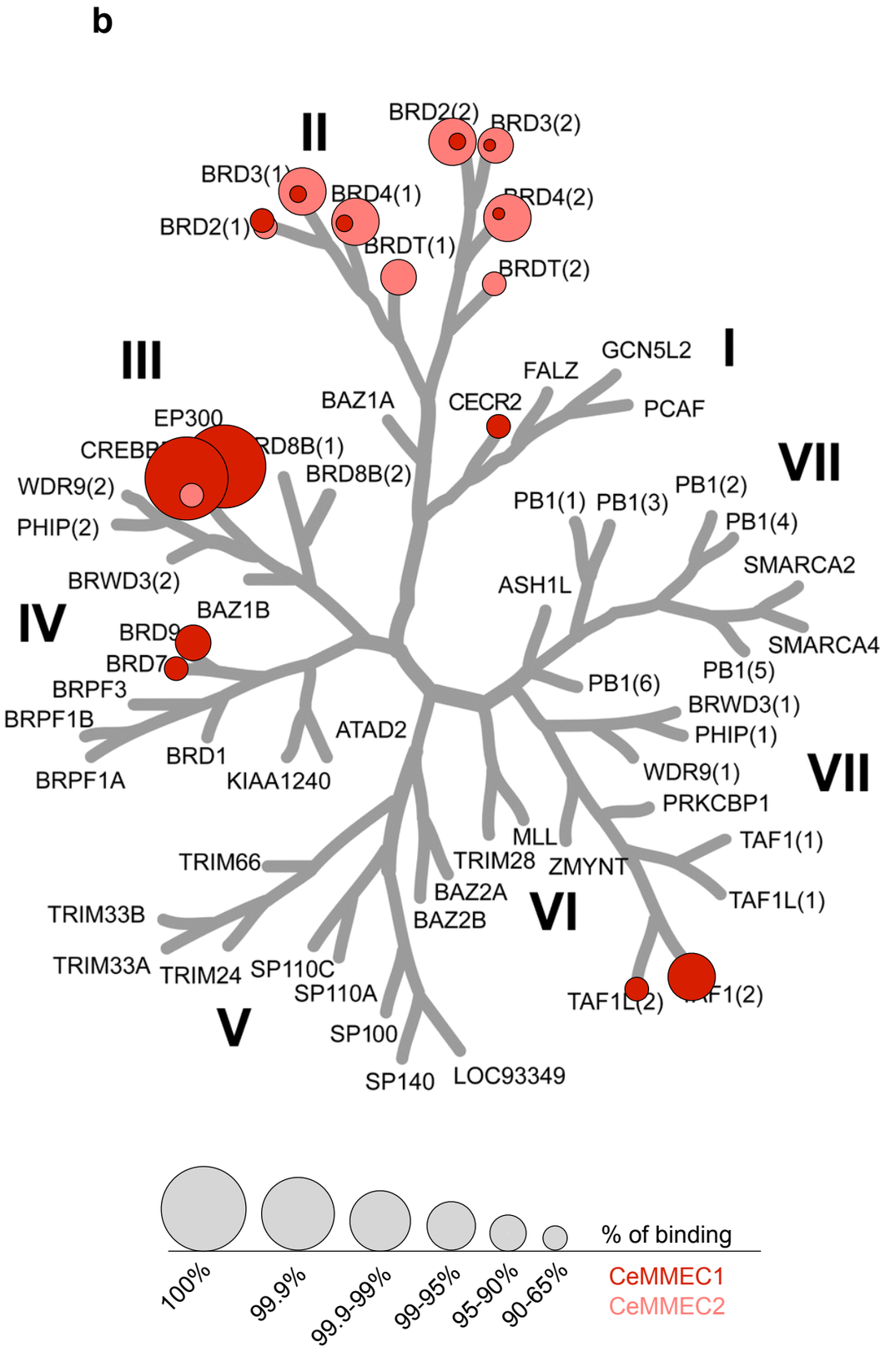

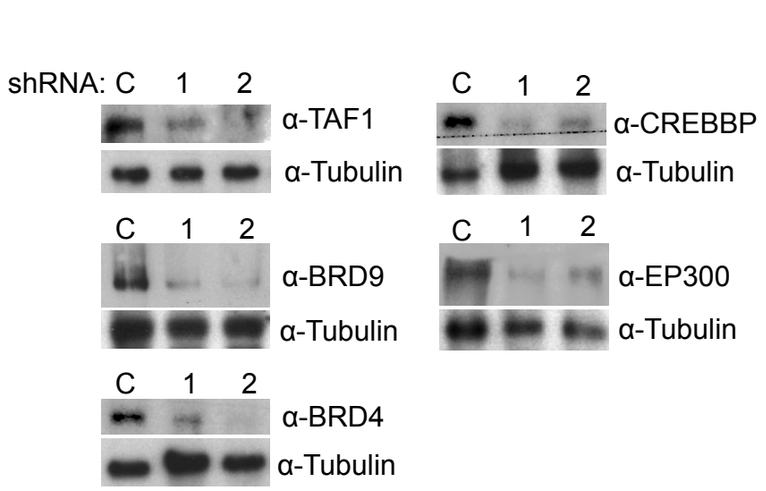

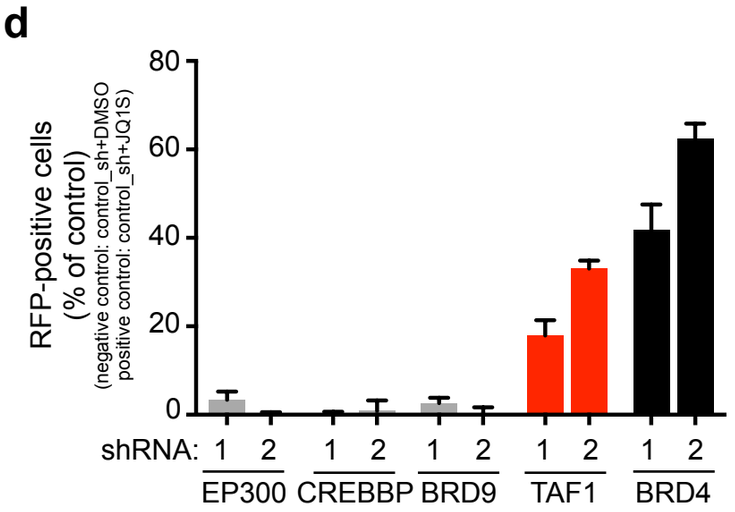

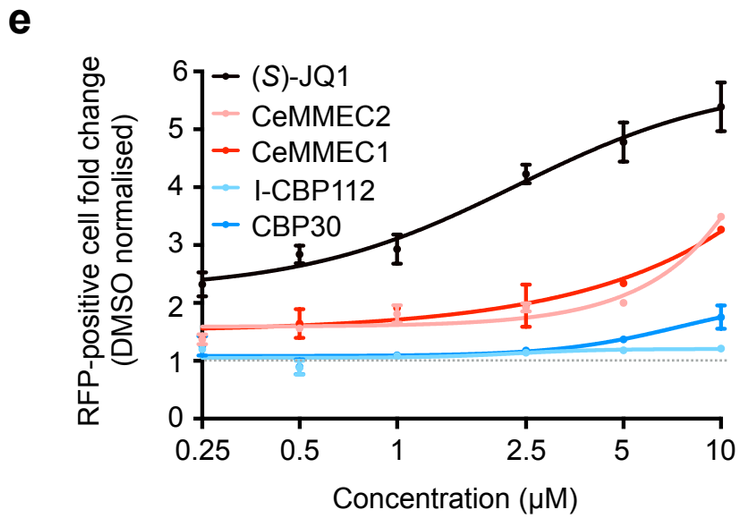

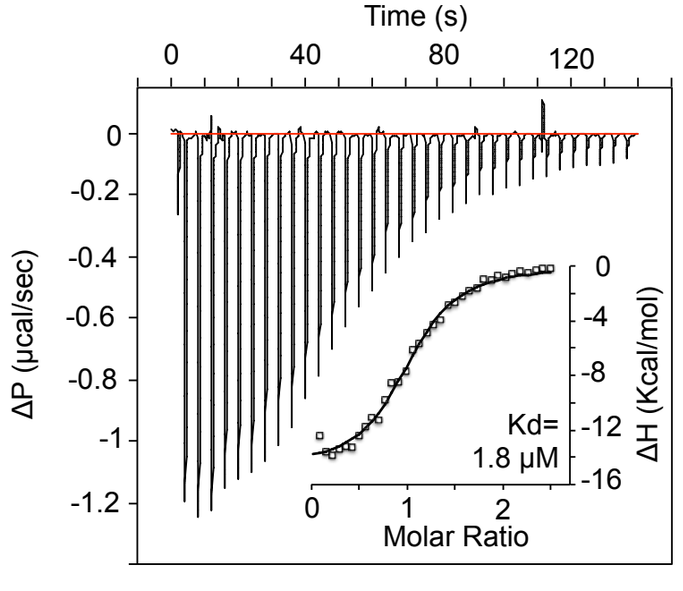

Sdelci et al; Fig.3

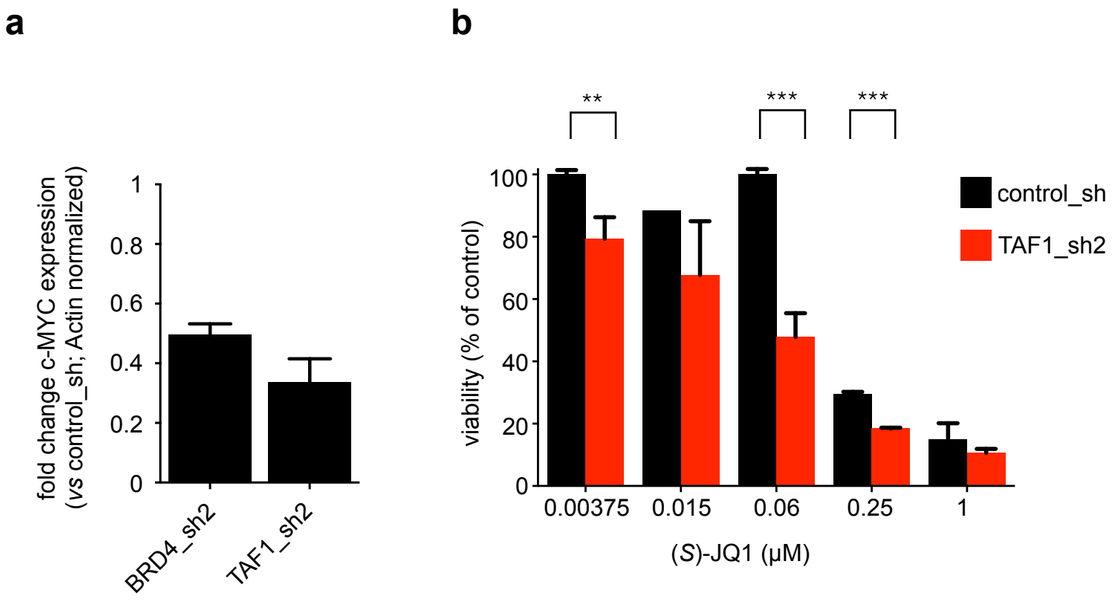

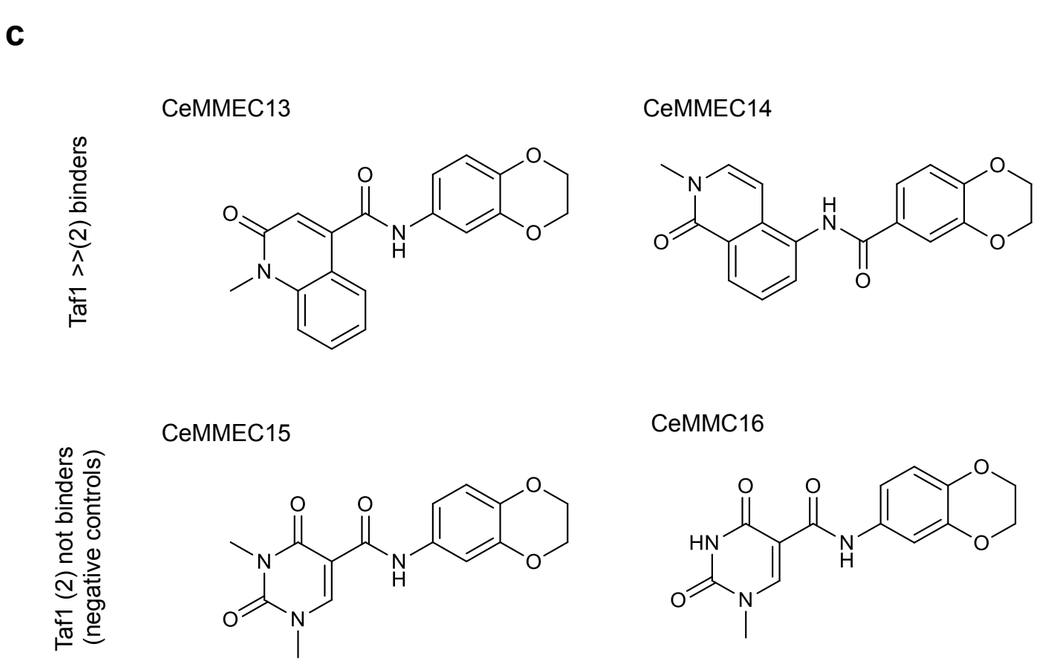

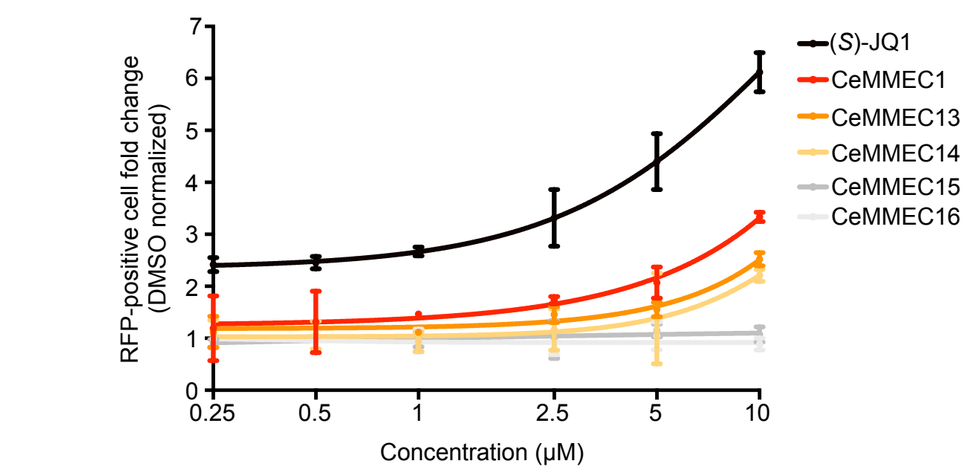

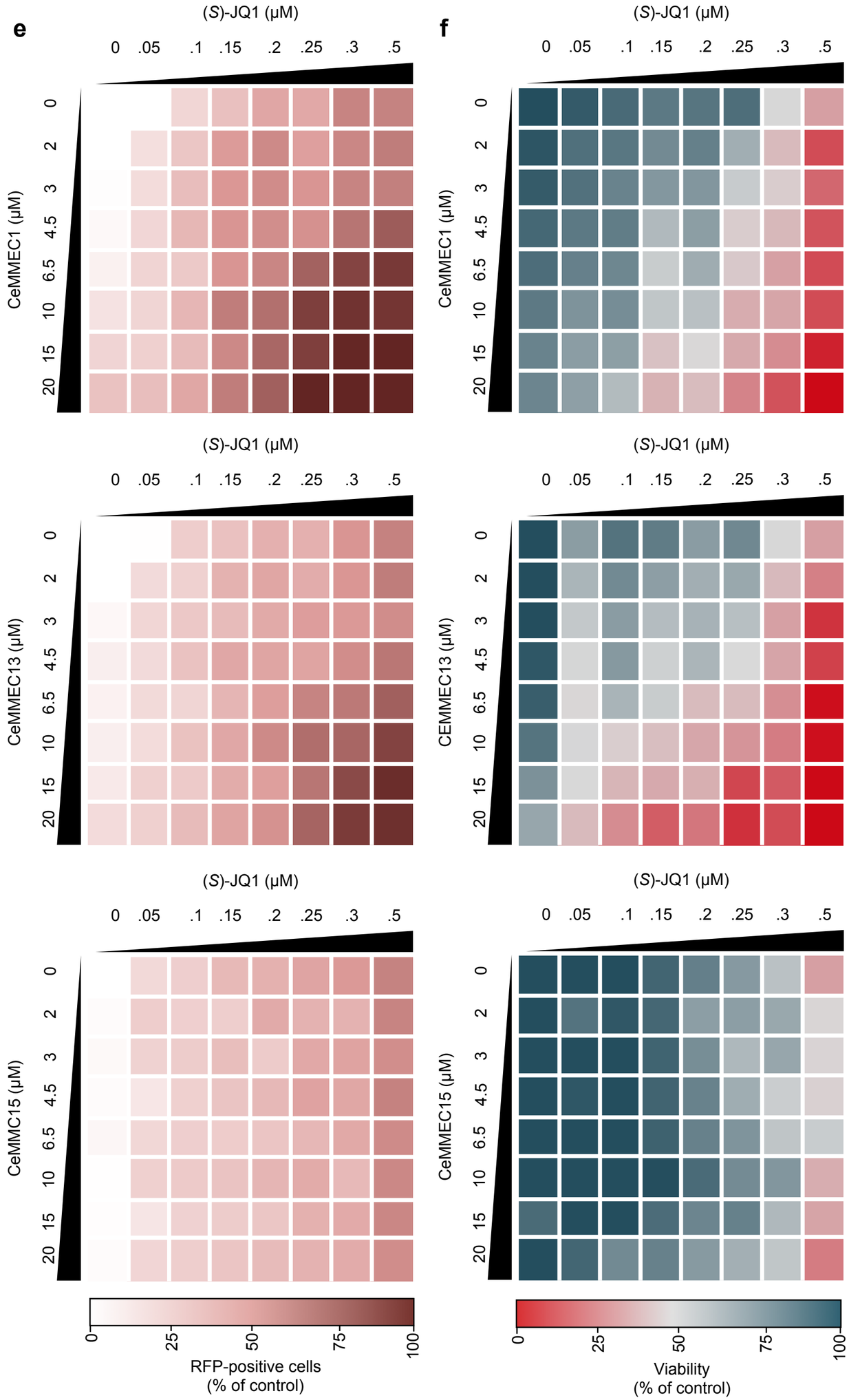

Sdelci et al; Fig.4